Characterization of Lanthanide Ion Binding to the EF-Hand Protein S100β by Luminescence Spectroscopy†

Dipankar Chaudhuri‡ and William DeW. Horrocks, Jr.*

152 Davey Laboratory, Department of Chemistry, The Pennsylvania State University, University Park, Pennsylvania 16802

Judith C. Amburgey§ and David J. Weber

Department of Biochemistry and Molecular Biology, University of Maryland School of Medicine, 108 North Greene Street, Baltimore, Maryland 21201

Received February 25, 1997; Revised Manuscript Received May 19, 1997⊗

ABSTRACT: S100β is a member of a group of low-molecular weight acidic calcium binding proteins widely distributed in the vertebrate nervous system containing two helix−loop−helix calcium binding motifs (sites I and II). In addition, S100β also has auxiliary Zn^{2+} binding sites that are distinct from the Ca^{2+} binding sites. Luminescence spectroscopy using Eu^{3+} and Tb^{3+} as spectroscopic probes for Ca^{2+} is used to characterize the Ca^{2+} binding sites of this protein. Eu^{3+}-bound S100β shows two distinct Eu^{3+} binding environments from both the excitation spectrum and Eu^{3+} excited state lifetimes. Eu^{3+} bound to the classical EF hand site II has a K_d of 660 ± 20 nM, whereas the dissociation constant for the pseudo-EF hand site I is significantly weaker. Lifetimes in H_2O and D_2O lead to the finding that there are four water molecules coordinated to the Eu^{3+} in the weakly binding site I and two water molecules to the tightly binding site II. Site II in S100β expectedly is very similar to high-affinity Ln^{3+} binding domains I and II in calmodulin. Eu^{3+} luminescence experiments with Zn^{2+}-loaded S100β show that the lifetime for Eu^{3+} in site I in Zn^{2+}-loaded S100β is significantly different than that in the absence of Zn^{2+}. Tyrosine-17-sensitized Tb^{3+} luminescence experiments indicate that the Tb^{3+} occupying the proximal weaker binding site I is sensitized, whereas Tb^{3+} in site II is not. The distance between sites I and II (15.0 ± 0.4 Å) in S100β was determined from Forster-type energy transfer in D_2O solutions containing bound Eu^{3+} donor and Nd^{3+} acceptor ions. For Zn^{2+}-S100β, the intersite distance is reduced to 13 ± 0.3 Å. Location of histidine-15 close to pseudo-EF site I suggests that Zn^{2+} binding likely changes the conformation of this site, causing a reduction of the intersite distance by approximately 2 Å.

The S100 group of small, acidic Ca^{2+} binding proteins is a highly conserved set found in the vertebrate nervous system (*1*−*4*). A principal member of the S100 protein family, S100β,[1] a neurite extension factor found in brain tissue, contains 91 amino acids (10.5 kDa) and is highly conserved in a variety of mammalian species (*3*−*5*).

Among the reported biological functions of S100β are effects on cytoskeletal systems, protein phosphorylation, and enzyme activities (*3*). In addition to these intracellular functions, a disulfide-linked dimer of S100β has neurotrophic activity on selected neuronal populations and mitogenic and morphogenic activity on astrocytes (*6*, *7*). The gene for S100β is mapped to the Down's syndrome region (bands 21q22.2 and 22.3) of human chromosome 21 (*8*), and S100β protein expression is increased in both Down's syndrome and Alzheimer's disease patients. S100β is localized primarily in activated astrocytes surrounding neuritic plaques, and the pattern of S100β overexpression in Alzheimer's disease correlates with the pattern of regional involvement by neuritic plaques (*9*), suggesting that an excess of S100β may signify a relationship between S100β levels and the neuropathology for these cognitive diseases.

According to models suggested by Kligman and Marshak (*6*), the biological functions of S100β and its corresponding disulfide-linked dimer, S100B(β-β), are related to the tightly regulated intra- and extracellular Ca^{2+} ion concentration. Each S100β subunit contains two helix−loop−helix calcium binding motifs, i.e. two classes of Ca^{2+} binding sites, one of high affinity (K_d = 20 μM) and one with a significantly reduced affinity (K_d = 200−500 μM) (*2*, *10*). It has been proposed that S100B($\beta\beta$) binds and modulates effector proteins in a manner similar to that of other Ca^{2+}-modulated proteins such as CaM. On the basis of sequence homologies with other Ca^{2+} binding proteins (i.e. calmodulin and troponin C), S100β is predicted to contain two EF-hand metal ion binding loops (*3*, *11*, *12*). While the C-terminal loop of S100β contains 12 residues, typical for a normal EF hand (site II), the N-terminal loop contains an EF hand with 14 residues, referred to as a pseudo-EF hand (site I), and

† This work was supported by the National Institutes of Health (Grant GM23599 to W.D.H. and Grant GM52071 to D.J.W.).

* To whom correspondence should be addressed. Phone: (814)-865-1191. Fax: (814)-865-3314.

‡ Present address: 208 Althouse Laboratory, Department of Biochemistry and Molecular Biology, The Pennsylvania State University, University Park, PA 16802.

§ Present address: Department of Chemistry, College of Wooster, Wooster, OH 44491.

⊗ Abstract published in *Advance ACS Abstracts,* July 15, 1997.

[1] Abbreviations: βME, β-mercaptoethanol; HEPES, 4-(2-hydroxyethyl)-1-piperazineethanesulfonic acid; K_d, dissociation constant; Ln^{3+}, generic convention for tripositive ions of the lanthanide ions; Nd-YAG, neodymium-yttrium aluminum garnet; S100β, subunit of dimeric S100B; S100B($\beta\beta$), dimeric S100B with noncovalent interactions at the dimer interface; S100B(β-β), dimeric S100B with disulfide bonds at the dimer interface; TDL, tunable dye laser.

S0006-2960(97)00435-2 CCC: $14.00

also contains four positively charged amino acids (*12*, *13*).

Among members of the S100 family of proteins, structural information exists for calbindin D_{9k} for which X-ray (*14*) and NMR structures (*13*, *15*, *16*) are available. However, calbindin is the protein with the least homology to the remainder of the S100 group, having only 27% identity with S100β. In addition, NMR structures have been reported for another S100 protein, calcyclin (*17*), and a high-resolution NMR structure has also been determined for apo-S100B($\beta\beta$) (*18*, *19*).

It has been proposed (*3*) that Ca^{2+} ion binding mediates a conformational change in these proteins, which exposes a patch of hydrophobic amino acid residues that are thought to be the site of effector protein binding. It is this S100−effector protein interaction that results in an alteration of effector protein activity and produces an intracellular response. According to this model, the conformational change occurring on binding to Ca^{2+} exposes hydrophobic domains of the protein to the solvent. These hydrophobic domains may then interact with similar hydrophobic domains on the effector protein and modulate its effects using various mechanisms, including blocking protein phosphorylation. The specificity of a particular S-100−effector protein interaction must then reside within the domains which are unique to individual S-100 proteins. Since Ca^{2+} binding to these proteins represents a major step in the regulation of their interaction with effector proteins, studies of the changes accompanying the binding of the Ca^{2+} ions to S100β (*3*−*20*) are extremely relevant. Furthermore, the recent NMR solution structure of rat apo-S100B($\beta\beta$) has led to further impetus for characterization of the Ca^{2+}-bound form of S100B. The orientation of the four helices within the apo-S100β subunit is such that a major conformational change in the C-terminal EF hand would be required for it to adopt a structure typical of the Ca^{2+}-bound state of calbindin D_{9k}, calcyclin, or calmodulin (*19*). In addition to binding Ca^{2+}, S100β reportedly binds two Zn^{2+} ions with high affinity at sites distant from the two Ca^{2+} sites (*10*), and part of the present investigation is centered around the effect of Zn^{2+} on the two distinct EF hand sites.

Studies which probe the S100β-bound metal ion are invaluable in determining the role of the metal ion in the structure and function of S100β which is the focus of the current study. The ability of certain lanthanide ions to luminesce at room temperature and their chemical similarity to the spectroscopically silent calcium ion have made them a widely used probe species for the study of calcium binding proteins (*21*−*25*). Excitation spectroscopy of the $^7F_0 \rightarrow {}^5D_0$ transition of Eu^{3+} ions bound to the calcium ion sites in EF hand proteins provides a wealth of information regarding the metal ion binding domains of proteins (for review, see ref 26). The focus of this study is characterization of the classes of metal ion binding sites, determination of the metal ion binding constants and the number of water molecules coordinated at each site, and measurement of the distance between the two metal ion sites. A preliminary abstract of this work has been presented (*27*).

MATERIALS AND METHODS

Materials. All chemicals were of the highest grade commercially available. Triply distilled nanopure water was used throughout. In order to reduce metal ion contamination, only acid-washed glassware and plasticware were used. All S100β solutions were buffered (50 mM HEPES at pH or pD 7.0 with no salt unless otherwise stated), and βME was employed (a 1.2 mM S100β stock contained 7.5 mM βME) to maintain the apo-S100β in the reduced state (prevent oxidative disulfide linkage formation). $EuCl_3 \cdot 6H_2O$ and $TbCl_3 \cdot 6H_2O$ were obtained from Aldrich Chemical Co. and were used without any further purification. All metal ion solutions were standardized by a complexometric technique (*28*).

S100β Protein Expression and Purification. To permit higher expression yields in *Escherichia coli*, the rat S100β gene was cloned into an overexpression plasmid, pRE1 containing a λP_1 promoter, and it was sequenced to verify the presence of the intact wild-type S100β gene. Next, the S100β gene was subcloned into the *Nde*I and *Bam*HI restriction sites of the pET11b plasmid (Novagen, Inc., Madison, WI) under the control of a T7 promoter, as previously described (*5*, *29*). The newly constructed plasmid was transferred into *E. coli* HB101 cells and sequenced again to verify the presence of the intact wild-type S100β gene. The purified, S100β-containing plasmid was then transferred into *E. coli* strain HMS174 (DE3) cells (Novagen, Inc.) which grow well on media with minimal nutrients. S100β from the cell lysates was purified to >98% homogeneity at 4 °C under reducing conditions (1 mM βME) as previously reported (*5*). Complete amino acid analyses (Analytical Biotechnology Sciences, Boston, MA) confirmed the composition of our S100β preparation.

Luminescence Measurements. Eu^{3+} excitation spectra, excited state lifetimes, and excitation intensities were recorded with a Continuum YG-581C pulsed Nd-YAG laser-pumped tunable TDL-50 dye laser as an excitation source. A mixture of rhodamine 590 and 610 dyes was used to access the $^7F_0 \rightarrow {}^5D_0$ transition of Eu^{3+} (577−581 nm) while monitoring the $^7F_0 \rightarrow {}^5D_2$ emission at 614 nm. The laser operates at 10 Hz, producing between 60 and 90 mJ/pulse with this dye mixture. Details of the laser system are published elsewhere (*30*).

Spectral peak fitting and luminescence decay analysis were achieved using the program PeakFit (Jandel Scientific). This program employs a nonlinear regression method based on the Marquardt algorithm. Luminescence decays were resolved into their component exponentials, yielding amplitudes, I_0, and lifetimes, τ, for each of the components. Excitation spectra were fit to individual peaks which can be described by a Lorentzian−Gaussian product function described elsewhere (*31*). For time-resolved experiments, luminescence decays were collected for a set time (normally 20 min) and corrected for laser power fluctuations during the course of the experiment.

Tb^{3+} Luminescence Experiments. Fluorescence emission and Tb^{3+} luminescence experiments were measured on a SPEX Fluorolog-2 spectrofluorimeter. The single Tyr 17 on S100β was excited at 275 nm, while its emission was scanned from 290 to 410 nm. Tyrosine-sensitized Tb^{3+} emission data were recorded by exciting the Tyr 17 at 275 nm and monitoring the Tb^{3+} emission at 545 nm. A 515 nm emission cutoff filter was used to avoid interference from harmonic doubling.

Eu^{3+}-S100β Binding Constant Measurements. Binding constants for Eu^{3+} were determined by plotting the amplitudes of the two component exponential functions (for the

two classes of Eu^{3+} binding sites) fit from the luminescence decay curves as a function of equivalents of added Eu^{3+}. The binding curve for the tightly binding classical EF hand site II was determined by fitting the luminescence decay curve corresponding to this site to a one-site binding model. Under the restrictions of our experimental conditions, it was not possible to evaluate the binding constant for the pseudo-EF hand site I as it was significantly weaker and allowed the use of a one-site binding model for site II. All binding constant measurements were done in triplicate, and the reported errors represent the rms devation of three trials.

Intermetal Ion Distance Measurements Using Forster Nonradiative Energy Transfer. Energy transfer measurements have been carried out between an energy donor ion, Eu^{3+}, and an energy acceptor ion, Nd^{3+}, in order to measure the distance between sites I and II on S100β, both in the absence and in the presence of Zn^{2+}. These distance measurements were done with a 19:1 ratio of Nd^{3+} to Eu^{3+} which was added to a total of 2 equiv of Ln^{3+} (relative to S100β monomer concentration), thus making sure that virtually every Eu^{3+} ion will have a Nd^{3+} ion neighbor. The calculations were carried out with both lifetimes arising from the two sites for independent verification of the distances obtained.

The experimental efficiency of energy transfer, E, is given by

$$E = 1 - \tau/\tau_0$$

where τ is the lifetime of Eu^{3+} in the presence of a neighboring energy acceptor and τ_0 in its absence. r, the distance between the ions, is given by

$$r = R_0[(1 - E)/E]^{1/6}$$

where R_0, the Forster critical distance for 50% energy transfer, is given by

$$(R_0)^6 = (8.75 \times 10^{-25})\kappa^2\phi\eta^{-4}J$$

where κ^2 is the dipole−dipole orientation factor ($^2/_3$ for metal ions), ϕ is the quantum yield of Eu^{3+} (estimated from τ_{H_2O}/τ_{D_2O}), η is the refractive index of the intervening medium (1.35 for our system), and J, the spectral overlap integral, is

$$J = \int \epsilon(\nu)F(\nu)\nu^{-4}\,d\nu / \int F(\nu)\,d\nu$$

where $\epsilon(\nu)$ is the molar absorptivity of the acceptor ion and $F(\nu)$ is the luminescence emission intensity of the donor ion.

RESULTS

Excitation Spectroscopy of the $^7F_0 \rightarrow {}^5D_0$ Transition of Eu^{3+} Bound to S100β

Figure 1 represents the $^7F_0 \rightarrow {}^5D_0$ excitation spectrum of 2 equiv of Eu^{3+} bound to S100β (10 μM). During the course of the titration up to 2 equiv, good fits of the spectra with two Lorentzian−Gaussian functions were obtained at and beyond 1 equiv; i.e. the spectra were resolved into two peaks with maxima at 579.20 nm (fwhm = 0.36 nm) and 579.49 nm (fwhm = 0.23 nm) corresponding to two distinct Eu^{3+} binding environments (two classes of binding sites). The fitting of the luminescence spectrum to two Lorentzian−Gaussian functions is further corroborated from the existence of two distinct Eu^{3+} excited state lifetimes discussed below.

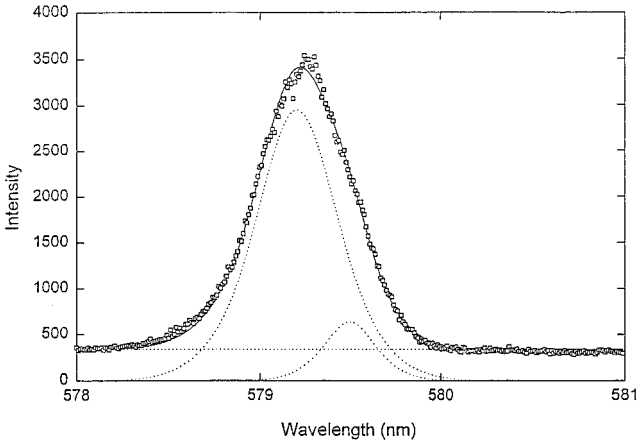

FIGURE 1: $^7F_0 \rightarrow {}^5D_0$ excitation spectrum of 2 equiv of Eu^{3+} in 10 μM S100β at pH 7.0 (50 mM HEPES). The spectrum is resolved into two peaks with maxima at 579.20 nm (fwhm = 0.36 nm) and 579.49 nm (fwhm = 0.23 nm).

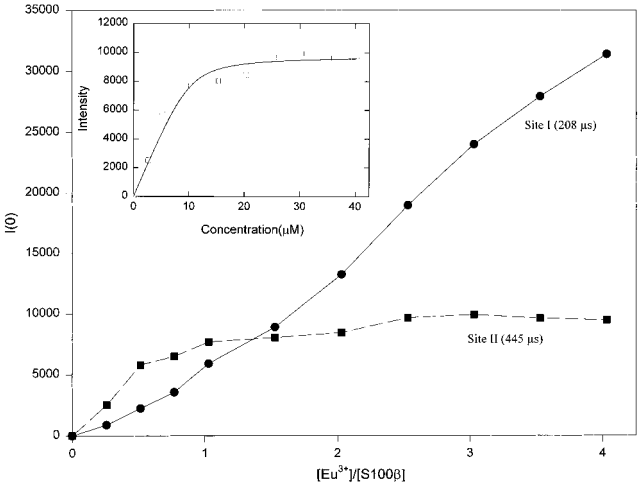

FIGURE 2: Amplitudes of the two-component exponential functions of Eu^{3+} luminescence curves (λ_{ex} = 579.3 nm) as a function of equivalents of added Eu^{3+} as the ion is titrated into apo-S100β (10 μM in 50 mM HEPES at pH 7.0). (Inset) Site II (445 μs component) amplitude data fitted to a single-site binding model yield a dissociation constant, K_d, of 660 nM.

Eu^{3+} Luminescence Decay Measurements

Additional information about the Eu^{3+} binding environments in S100β is obtained by (a) recording the luminescence decays at the excitation maximum as Eu^{3+} is titrated into the protein and (b) recording the time course of the luminescence decay separately in H_2O and D_2O solutions. Figure 2 shows the amplitudes, I_0, of the two-component exponential functions of the luminescence decay curves (λ_{ex} = 579.3 nm) as a function of added Eu^{3+} as the ion is titrated into apo-S100β (in H_2O buffer). Two distinct Eu^{3+} excited state lifetimes of 445 ± 30 and 208 ± 20 μs are observed. On the basis of this titration, we assign the 445 μs component to site II, the classical EF hand site, since it is saturated at a low metal ion concentration. In addition, this lifetime is very similar to the high-affinity Ln^{3+} binding domains I and II in calmodulin (441 μs) (*23*). The 208 μs component is assigned to the pseudo-EF hand site I, which becomes occupied at higher metal ion concentrations. This assignment

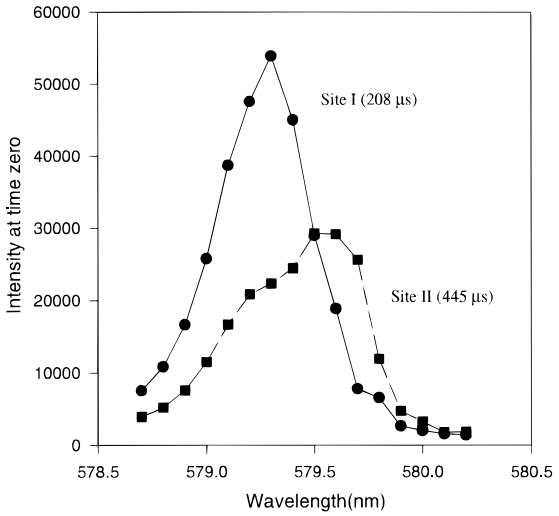

FIGURE 3: Time-resolved spectrum of Eu^{3+} in 10 μM apo-S100β at pH 7.0 (50 mM HEPES). Intensities at time zero (I_0) of the 208 and 445 μs lifetimes are plotted as a function of excitation wavelength.

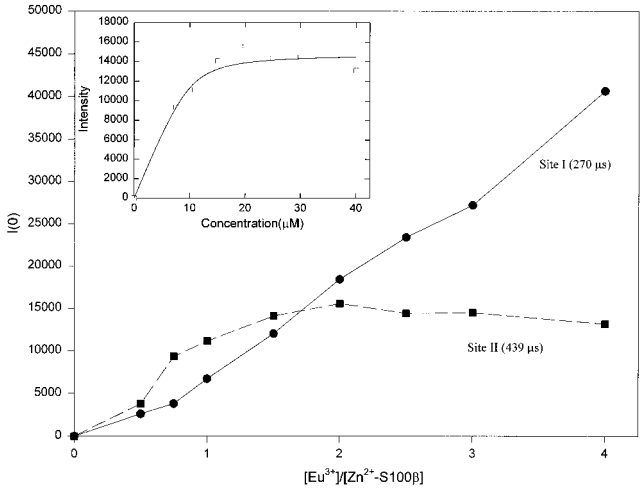

FIGURE 4: Amplitudes of the two-component exponential functions of Eu^{3+} luminescence curves (λ_{ex} = 579.3 nm) as a function of equivalents of added Eu^{3+} as the ion is titrated into Zn^{2+}-loaded S100β (10 μM in 50 mM HEPES at pH 7.0 with 4 equiv of Zn). (Inset) Site II (439 μs component) amplitude data fitted to a single-site binding model yield a dissociation constant, K_d, of 726 nM.

of sites is further corroborated by the time-resolved spectrum for Eu^{3+}-S100β and sensitized Tb^{3+} luminescence experiments discussed below.

Determination of Binding Constants for Eu^{3+}-S100β. From the experiment described in Figure 2 (i.e. I_0 values of the component exponentials as a function of added Eu^{3+}), it is apparent that the τ = 445 μs component corresponds to the tightly binding site (site II) in S100β. These data fit to a single-independent site binding model yield a dissociation constant K_d of 660 $\pm$ 20 nM. The τ = 208 μs component is assigned to the weakly binding pseudo-EF hand site I, but due to experimental constraints (the binding curve does not reach saturation before precipitation occurs), we were not able to measure the dissociation constant for this site.

Time-Resolved Spectrum for Eu^{3+}-S100β. In order to probe further the two distinct Eu^{3+}-binding environments in S100β and to find out where in the excitation spectrum the different lifetimes contribute, a time-resolved spectrum was recorded for 2 equiv of Eu^{3+} bound to S100β. In this experiment, luminescence decays were recorded at 0.1 nm increments along the excitation spectrum. The amplitudes of the component exponentials, I_0, are plotted as a function of excitation wavelength to produce a spectrum as shown in Figure 3. The 208 μs component peak is centered at about 579.2 nm, while the 445 μs component is centered around 579.5 nm, confirming that the 208 μs component is from site I and the latter component is from site II.

Number of Water Molecules Coordinated to the Two Eu^{3+} Binding Sites. Additional information about the environment of Eu^{3+} can be obtained by recording the time course of luminescence decay separately in H_2O and D_2O solutions. It has been shown by Horrocks and Sudnick (*32*) that the number of water molecules, q, in the first coordination sphere of Eu^{3+} is given by

$$q = 1.05(\tau^{-1}_{H_2O} - \tau^{-1}_{D_2O})$$

where τ^{-1} is the reciprocal of the excited state lifetime (ms^{-1}) in the solvent indicated. In D_2O solution, the corresponding Eu^{3+} excited state lifetimes are 950 $\pm$ 40 μs for site I and 2140 $\pm$ 30 μs for site II. By using the above equation, the number of innersphere-coordinated water molecules is calculated to be 3.9 $\pm$ 0.5 for site I (pseudo-EF site) and 1.9 $\pm$ 0.5 for site II (EF hand site). The two water molecules coordinated to Eu^{3+} at site II of S100β are also the same as the corresponding sites in calmodulin (*23*). On the other hand, expectedly, the considerably more weakly binding pseudo-EF site (site I) (K_d not measurable under our experimental conditions) has four water molecules coordinated to the Eu^{3+}, and hence fewer coordinating atoms from the protein.

Effect of Zn^{2+} on Eu^{3+} Binding to S100β

In addition to binding Ca^{2+}, S100β reportedly binds up to four Zn^{2+} ions with high affinity (K_d = 0.1−1.0 μM) at sites different from Ca^{2+} (*10*, *33*). Qualitative data from fluorescence, UV differential spectroscopy, and CD studies indicate that Zn^{2+} ion binding, like Ca^{2+} binding, induces changes in the S100β conformation and that Ca(II) ion binding affinity is increased in the presence of Zn^{2+} (*10*). Our experiments are directed toward probing the effect of Zn^{2+} on Eu^{3+} binding to S100β via Eu^{3+} excited state lifetimes.

Figure 4 shows the amplitudes, I_0, of the two-component exponential functions of Eu^{3+} luminescence decay curves (λ_{ex} = 579.3 nm) as a function of added Eu^{3+} as this ion is titrated into Zn^{2+}-loaded S100β (10 μM in 50 mM HEPES at pH 7.0 with 4 equiv of Zn^{2+}). The 4 equiv of Zn^{2+} was added to ensure that all the Zn^{2+} sites were filled prior to sequential Eu^{3+} addition. It should be pointed out that initial experiments were done with 6 equiv of Zn^{2+} (excess) and the results (data not shown) were identical to the data discussed hereafter. In H_2O solution, the Zn^{2+}-loaded protein has two distinct Eu^{3+} excited state lifetimes of 270 $\pm$ 20 μs (for site I) and 439 $\pm$ 30 μs (for site II) versus 208 $\pm$ 20 and 445 $\pm$ 30 μs in the absence of Zn^{2+}. On the basis of these lifetime values and the fact that the dissociation constant for Eu^{3+} bound to site II in Zn^{2+}-S100β is determined to be 726 $\pm$ 20 nM, there does not seem to be any significant influence of Zn^{2+} when Eu^{3+} binding to site II is considered. Because of experimental constraints, the

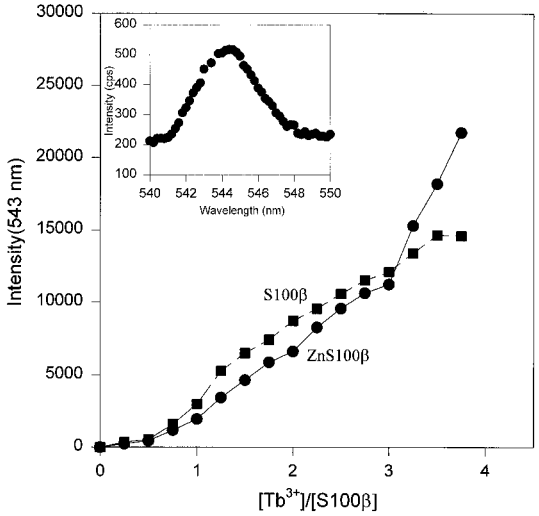

FIGURE 5: Tyrosine-sensitized Tb^{3+} emission at 544.4 nm (λ_{ex} = 280 nm) as a function of total equivalents of Tb^{3+} added to apo- and Zn-loaded S100β both at 10 μM in 50 mM HEPES at pH 7.0. (Inset) Tb^{3+} emission spectrum from 540 to 555 nm for 2 equiv of Tb^{3+} in 10 μM apo-S100β.

dissociation constant for site I could not be determined. However, the lifetime value of 270 μs for site I in the Zn^{2+}-loaded protein is somewhat different from the corresponding lifetime (208 μs) for the pseudo-EF hand weak site in the absence of Zn^{2+}. These data suggest that Zn^{2+} introduces conformational changes in the protein in the vicinity of site I of S100β.

Sensitized Tb^{3+} Luminescence Experiments: Sequence of Lanthanide Ion Binding in S100β

Tyrosine-sensitized Tb^{3+} luminescence titrations were performed to determine the order in which lanthanide ions occupy the binding sites in S100β and Zn^{2+}-loaded S100β. Sequence analysis of S100β shows that there is a single tyrosine residue at position 17 near the N-terminal Ca^{2+} ion binding site (site I, pseudo-EF). Figure 5 shows the tyrosine-sensitized Tb^{3+} emission at 544.5 nm (λ_{ex} = 280 nm) as a function of added Tb^{3+} to apo- and Zn-loaded S100β. These experiments with both S100β and ZnS100β indicate that the Tb^{3+} occupying the proximal more weakly binding site I is sensitized by tyrosine 17 whereas the distant more tightly bound Eu^{3+} in site II is not. The plot clearly indicates that the previously assigned tightly binding classical EF hand site II is occupied first (no appreciable Tb^{3+}-sensitized emission prior to the addition of 1 equiv) followed by occupancy of the more weakly binding pseudo-EF hand site I (sensitized Tb^{3+} emission after 1 equiv of added Tb^{3+}).

Forster-Type Nonradiative Energy Transfer Distance Measurement between Eu(III) and Nd(III) in Sites I and II

If a luminescent Eu^{3+} ion is placed in proximity to another ion whose absorption spectrum overlaps the emission spectrum of Eu^{3+}, Forster-type nonradiative energy transfer can take place. From the efficiency of this transfer, it is possible, in principle, to measure the distance, *r*, between these two ions, provided that no other energy transfer mechanism is operative. Forster-type energy transfer has been used to measure organic fluorophore−transition metal ion (*34*), intrinsic fluorophore−lanthanide metal ion (*23*, *35*), lanthanide ion−transition metal ion (*36*, *37*), and inter-

Table 1: Distance Measurement Data

	τ_0 (ms)[a]	τ (ms)[b]	E[c]	ϕ[d]	R_0 (Å)[e]	r (Å)[f]
S100β						
site I	0.95	0.82	0.13	0.78	10.9	15.2
site II	2.14	1.91	0.11	0.78	10.9	14.9
ZnS100β						
site I	0.78	0.58	0.25	0.78	10.9	13.1
site II	1.66	1.22	0.26	0.78	10.9	13.0

[a] τ_0 = lifetime in the absence of the acceptor (in D_2O). [b] τ = lifetime in the presence of the acceptor (in D_2O). [c] E = efficiency of energy transfer. [d] ϕ = quantum yield (the quantum yield of the Eu^{3+} aqua ion in D_2O solution is 0.78). [e] R_0 = critical distance for 50% energy transfer. [f] r = intermetal ion distance.

lanthanide ion distances in proteins (*21*, *22*, *38*−*40*). In order to achieve this in CaM, where sites I and II bind with nearly equal affinities, Horrocks and Tingey (*22*) used a 1:19 Eu^{3+}/Nd^{3+} metal ion mixture to avoid the presence of two Eu^{3+} ions in any one EF hand pair (that is, to ensure that nearly every Eu^{3+} ion in the protein has a Nd^{3+} ion in the neighboring site). Although the Ln^{3+} ion binding affinities of site I and site II in S100β are significantly different, we used the 1:19 metal ion mixture to measure the distance between sites I and II in S100β in the presence and absence of Zn^{2+}.

Table 1 lists the parameters relevant to the calculation of the distance between sites I and II. κ^2, the dipole−dipole orientation factor, was taken to be $^2/_3$, the value for the isotropic case. *J*, the spectral overlap integral, was taken to be 1.4×10^{-17} cm^{-6} mol^{-1} determined by Horrocks and Tingey (*22*) for Eu^{3+} and Nd^{3+} in CaM. Since our energy transfer measurements were done in D_2O, we used a ϕ_{D_2O} of 0.78 in our calculation (*41*).

The distance between sites I and II in S100β was measured by observing the luminescent decay of a 10 μM solution of this protein with 4 equiv of Eu^{3+} alone (to ensure maximum loading of weak site I) or with a Eu/Nd (1:19) mixture (4 equiv of total metal ion). Independent measurements of unquenched and quenched lifetimes for both sites I and II were done for independent verification of the intersite distance. For S100β, in the absence of Nd^{3+}, the lifetimes corresponding to sites I and II are 0.95 ± 0.04 and 2.14 ± 0.03 ms, respectively. In the presence of Nd^{3+}, these two lifetimes are 0.82 ± 0.03 and 1.91 ± 0.03 ms, respectively, and this quenching of the lifetimes by Forster nonradiative energy transfer leads to an intersite distance of 15.0 ± 0.04 Å. Although this distance is somewhat greater than what is found in CaM (11.5 Å between sites III and IV) (*42*), recent NMR structural data for apo-S100B (*19*) indicate that this distance is well within the range expected for S100β. For ZnS100β, the intersite distance is found to be 13.0 ± 0.03 Å, suggesting that Zn^{2+} introduces conformational changes in the protein whereby the intersite distance is reduced perhaps by changes in the vicinity of the pseudo-EF weak site (site I). This is corroborated by the observation that the lifetimes of Eu^{3+} bound to site I in the absence and presence of Zn^{2+} are different (208 versus 270 μs).

DISCUSSION

The recent multidimensional solution NMR structure of the apo-S100B (*19*) dimer shows that the four helices within each apo-S100β subunit adopt a unicornate-type four-helix bundle, with helix I protruding from the parallel bundle of

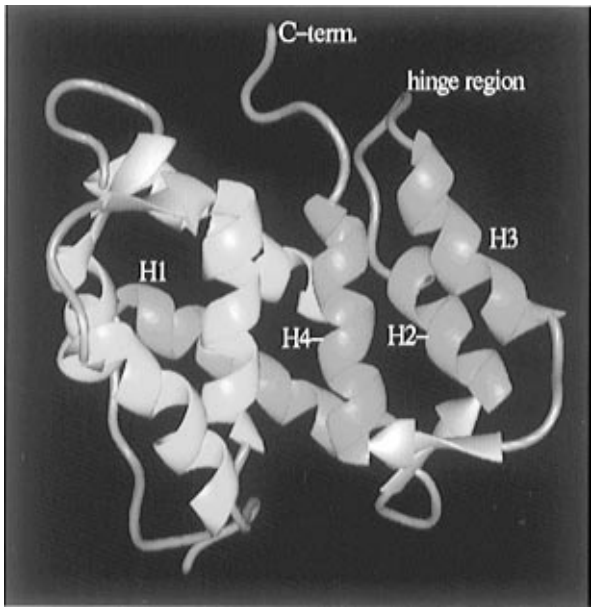

FIGURE 6: Ribbon diagram of apo-S100B($\beta\beta$) illustrating the X-type four-helix bundle (two pairs of crossing helices) at the dimer interface and the unicornate-type four-helix bundle (one helix forms a large angle with the others) within each subunit. The small β-sheet of each apo-S100β (pink) and the loops (gray) are also known (Drohat et al., 1996).

helices II−IV. The orientation of helix III relative to helices I, II, and IV in each subunit differs significantly from that known for other Ca^{2+} binding proteins. The interhelical angle, Ω, observed in the C-terminal EF hand of apo-S100β is −142°, whereas Ω ranges from 118 to 145° in the apo state and from 84 to 128° in the Ca^{2+}-bound state for the EF hands of calbindin D_{9k}, calcyclin, and calmodulin (*19*). Thus, a significant conformational change in the C-terminal EF hand would be required for it to adopt a structure typical of the Ca^{2+}-bound state in these prototypical EF hand proteins. Luminescence spectroscopy of the Eu^{3+} bound to site II of S100β indicates that the coordination sphere of Eu^{3+} bound to site II of S100β appears to be very similar to that of Eu^{3+} bound to calmodulin. In fact, both the lifetime of 445 μs (for site II) and the two innersphere-coordinated water molecules at this site are very similar to those of the high-affinity Ln^{3+} binding domains I and II in calmodulin (441 μs, two coordinated water molecules) (*23*). In S100β, six ligands at site II are provided by the protein as is the case for Ln^{3+} binding sites I and II in calmodulin. It is therefore suggested that apo-S100β goes through a dramatic conformational change upon metal addition (including alignment of the four liganding residues D61, D63, D65, and E72 at the *X*, *Y*, *Z*, and $-Z'$ positions, respectively) to obtain a coordination sphere at site II similar to that of the metal ion bound to sites I and II in calmodulin. This conformational change is less dramatic for CaM and other EF hand proteins where only the bidentate glutamate residue in the $-Z$ and the $-Z'$ positions is realigned upon Ca^{2+} binding. This interpretation suggests that the k_{on} rate for metal ion binding to S100β (at site II) may be smaller than that for sites I and II in CaM, which explains the smaller affinity for Ca^{2+} at site II (20−50 μM in S100β versus 1 μM in CaM) as compared to the corresponding sites I and II in CaM (*43*). This difference in affinity is also mimicked in the corresponding Ln^{3+} binding affinities of 660 nM for site II in S100β and 1.0 nM for the Ln^{3+} tightly binding domains I and II in calmodulin (*23*).

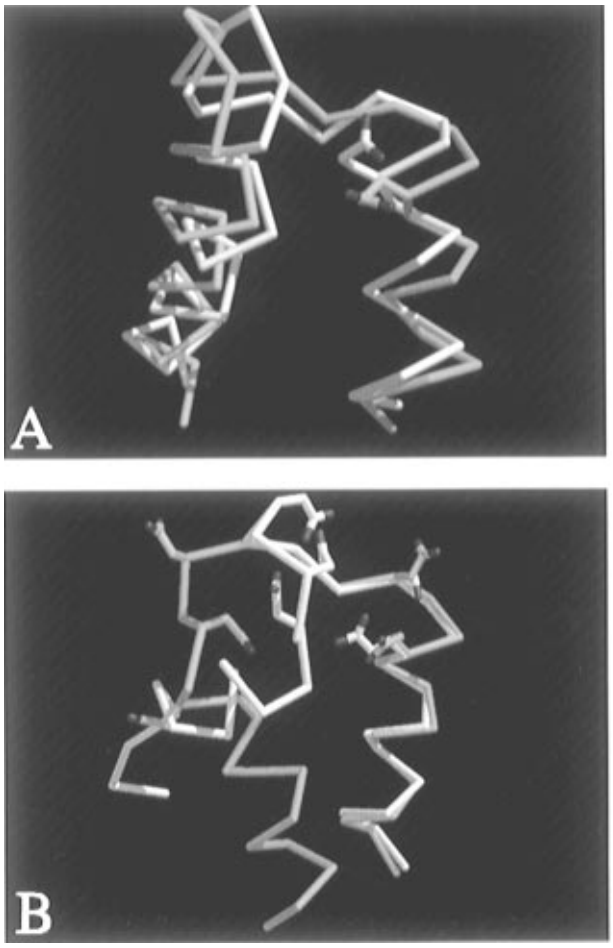

FIGURE 7: Comparison of the EF hands of apo-S100B($\beta\beta$) and apocalbindin (A). Residues A6−L40 of the (N-terminal) pseudo-EF hand in apo-S100β (blue) are superimposed (Cα) with the analogous residues, K5−F39, in the pseudo-EF hand of calbindin (white). (B) Residues Q50−A83 from the (C-terminal) typical EF hand in apo-S100B($\beta\beta$) (blue) are superimposed (Cα) with the homologous residues (L49−Q78) of the typical EF hand in apocalbindin D_{9k} (white). The overlay was performed by aligning residues 67−82 of apo-S100B ($\beta\beta$) with residues 63−78 of apocalbindin D_{9k}, which include the C-terminal β-strand and helix IV from each protein (Drohat et al., 1996).

Our results show that for the pseudo-EF hand site I in S100β there are four water molecules coordinated to the inner sphere of Eu^{3+} at this site (consistent with its weak binding affinity) leaving five coordination sites to be filled by residues from the protein. On the basis of the sequence homology between the pseudo-EF hands of S100β and calbindin D_{9k} (see Figure 7), it is predicted that the carbonyl atoms of residues S18, E21, D23, and K26 and the carboxylate oxygen atoms of E31 are involved in the coordination to Ca^{2+}; however, our results conclusively establish that five (rather than six) coordination sites come from S100β, and since all the relevant coordinating atoms in the above residues are all clustered within a 5 Å radius sphere in the apo structure of S100B($\beta\beta$), it is difficult to predict which of these residues does not ligate in the holo state.

The intersite distance (from site I to site II) of 15.0 ± 0.4 Å in S100β is somewhat longer than that found in similar Ca^{2+} binding proteins like calmodulin (11.5 Å between sites III and IV and 12.1 Å between sites I and II), but this is

well within the expected range for S100β on the basis of the location of the residues that are coordinated to the metal ion at these two sites. It should also be pointed out that, although S100B exists as a natural dimer in the concentration domain of our experiment (K_d < 1 nM) (*44*), the above intersite distance of 15.0 ± 0.4 Å is within the monomer as the distance between similar sites across the dimer is in the range of 30−40 Å on the basis of the apo-S100B($\beta\beta$) structure. Therefore, all (>99%) of the energy transfer is within a single subunit due to the r^6 dependence of this phenomenon. The reduction of the intersite distance to 13 Å in Zn-S100β is perhaps caused by a conformational realignment of relevant residues in the vicinity of the pseudo-EF hand site I. As mentioned earlier, this is further corroborated by the observation that the lifetimes of Eu^{3+} bound to site I in the absence and presence of Zn are different (208 versus 270 μs). The high-resolution NMR structure of apo-S100B does show the localization of His 15 and His 25 (possible Zn^{2+} binding ligands) in the vicinity of the pseudo-EF site I which probably suggests that Zn^{2+} binding is causing a conformational change around site I leading to a reduction of the intersite distance by approximately 2 Å.

REFERENCES

1. Moore, B. E. (1965) *Biochem. Biophys. Res. Commun. 19*, 739−744.
2. Hilt, D. C., and Kligman, D. (1988) *Trends Biochem. Sci. 13*, 437−443.
3. Hilt, D. C., and Kligman, D. (1991) in *Novel Calcium-Binding Proteins* (Heizmann, C., Ed.) pp 65−103, Springer, Berlin.
4. Donato, R. (1991) *Cell Calcium 12*, 713−726.
5. Amburgey, J. C., Abildgaard, F., Starich, M. R., Shah, S., Hilt, D. C., and Weber, D. J. (1995) *J. Biomol. NMR 6*, 171−179.
6. Kligman, D., and Marshak, D. (1985) *Proc. Natl. Acad. Sci. U.S.A. 82*, 7136−7139.
7. Barger, S. W., Wolchok, S. R., and Van Eldik, L. J. (1992) *Biochim. Biophys. Acta 1160*, 105−112.
8. Allore, R., O'Hanlon, D., Price, R., Neilson, K., Willard, H. F., Cox, D. R., Marks, A., and Dunn, R. J. (1988) *Science 239*, 1311−1313.
9. Van Eldik, L. J., and Griffin, W. S. T. (1994) *Biochim. Biophys. Acta 1223*, 398−403.
10. Baudier, J., Glasser, N., and Gerard, D. (1986) *J. Biol. Chem. 261*, 8192−8203.
11. Kretsinger, R. H. (1980) *CRC Crit. Rev. Biochem. 8*, 119−174.
12. Strynadka, N. C. J., and James, M. N. G. (1989) *Annu. Rev. Biochem. 58*, 951−988.
13. Skelton, N. J., Kordel, J., Akke, M., Forsen, S., and Chazin, W. J. (1994) *Nat. Struct. Biol. 1*, 239−245.
14. Szebenyi, D. M. E., and Moffat, K. (1986) *J. Biol. Chem. 261*, 8761−8767.
15. Akke, M., Drakenburg, T., and Chazin, W. J. (1992) *Biochemistry 31*, 1011−1020.
16. Kordel, J., Skelton, N. J., Akke, M., and Chazin, W. J. (1993) *J. Biol. Chem. 231*, 711−734.
17. Potts, B. C. M., Smith, J., Akke, M., Macke, T. J., Okazaki, K., Hidaka, H., Case, D. A., and Chazin, W. J. (1995) *Nat. Struct. Biol. 2*, 790−796.
18. Kilby, P. M., Van Eldik, L. J., and Roberts, G. C. K. (1995) *FEBS Lett. 363*, 90−96.
19. Drohat, A. C., Amburgey, J. C., Abildgaard, F., Starich, M. R., Baldisseri, D., and Weber, D. J. (1996) *Biochemistry 35*, 11577−11588.
20. Zimmer, D. B., Cornwall, E. H., Lander, A., and Song, W. (1995) *Brain Res. Bull. 37*, 417−429.
21. Mulqueen, P., Tingey, J. M., and Horrocks, W. D., Jr. (1985) *Biochemistry 24*, 6639−6645.
22. Horrocks, W. D., Jr., and Tingey, J. M. (1988) *Biochemistry 27*, 413−419.
23. Bruno, J., Horrocks, W. D., Jr., and Zauhar, R. J. (1992) *Biochemistry 31*, 7016−7026.
24. Burroughs, S. E., Horrocks, W. D., Jr., Ren, H., and Klee, C. B. (1994) *Biochemistry 33*, 10428−10436.
25. Bruno, J., Horrocks, W. D., and Beckingham, K. (1996) *Biophys. Chem. 63*, 1−16.
26. Horrocks, W. D., Jr. (1993) *Methods Enzymol. 226*, 495−538.
27. Chaudhuri, D., Horrocks, W. D., Jr., Amburgey, J. C., and Weber, D. J. (1996) *Biophys. J. 70*, A211.
28. Fritz, J. S., Oliver, R. T., and Pietrzyk, D. J. (1958) *Anal. Chem. 30*, 1111−1114.
29. Abeygunawardene, C., Weber, D. J., Frick, D. N., Bessner, M. J., and Mildvan, A. S. (1993) *Biochemistry 32*, 13071−13080.
30. Frey, S. T., Chang, C. A., Carvalho, J. F., Varadarajan, A., Schultze, L. H., Pounds, K. L., and Horrocks, W. D., Jr. (1994) *Inorg. Chem. 33*, 2882−2889.
31. McNemar, C. W., and Horrocks, W. D., Jr. (1989) *Appl. Spectrosc. 43*, 816−821.
32. Horrocks, W. D., Jr., and Sudnick, D. R. (1979) *J. Am. Chem. Soc. 101*, 334−340.
33. Van-Eldik, L. J., Staecker, J. L., and Winningham-Major, F. (1988)*J. Biol. Chem. 263*, 7830−7837.
34. Latt, S. A., Auld, D. S., and Vallee, B. L. (1972) *Biochemistry 11*, 3015−3022.
35. Horrocks, W. D., Jr., and Collier, W. E. (1981) *J. Am. Chem. Soc. 103*, 2856−2860.
36. Horrocks, W. D., Jr., Holmquist, B., and Vallee, B. L. (1975) *Proc. Natl. Acad. Sci. U.S.A. 72*, 4764−4768.
37. Meares, C. F., and Ledbetter, J. E. (1977) *Biochemistry 16*, 5178−5180.
38. Wang, C.-L. A., Tao, T., and Gergely, G. (1982) *J. Biol. Chem. 258*, 8372−8375.
39. Snyder, A. P., Sudnick, D. R., Arkle, V. K., and Horrocks, W. D., Jr. (1981) *Biochemistry 20*, 3334−3339.
40. Rhee, M. J., Sudnick, D. R., Arkle, V. K., and Horrocks, W. D., Jr. (1981) *Biochemistry 20*, 3328−3333.
41. Haas, Y., and Stein, G. (1971) *J. Phys. Chem. 75*, 3668−3677.
42. Babu, Y. S., Bugg, C. E., and Cook, W. J. (1988) *J. Mol. Biol. 254*, 191−204.
43. Crivici, A., and Ikura, M. (1995) *Annu. Rev. Biophys. Biomol. Struct. 24*, 85−116.
44. Drohat, A. C., Nenortas, E., Beckett, D., and Weber, D. J. (1997) *FASEB J.* (in press).

BI9704358